Neuron
Article

Mind Bomb 1-Expressing Intermediate Progenitors Generate Notch Signaling to Maintain Radial Glial Cells

Ki-Jun Yoon,[1] Bon-Kyoung Koo,[1] Sun-Kyoung Im,[1] Hyun-Woo Jeong,[1] Jaewang Ghim,[1] Min-chul Kwon,[1] Jin-Sook Moon,[1] Takaki Miyata,[2] and Young-Yun Kong[1,*]
[1]Division of Molecular and Life Sciences, Pohang University of Science and Technology, Pohang, Kyungbuk, 790-784, South Korea
[2]Department of Anatomy and Cell Biology, Nagoya University Graduate School of Medicine, 65 Tsurumai, Showa, Nagoya, Aichi 466-8550, Japan
*Correspondence: ykong@postech.ac.kr
DOI 10.1016/j.neuron.2008.03.018

SUMMARY

Notch signaling is critical for the stemness of radial glial cells (RGCs) during embryonic neurogenesis. Although Notch-signal-receiving events in RGCs have been well characterized, the signal-sending mechanism by the adjacent cells is poorly understood. Here, we report that conditional inactivation of *mind bomb-1* (*mib1*), an essential component for Notch ligand endocytosis, in mice using the *nestin* and *hGFAP* promoters resulted in complete loss of Notch activation, which leads to depletion of RGCs, and premature differentiation into intermediate progenitors (IPs) and finally neurons, which were reverted by the introduction of active Notch1. Interestingly, Mib1 expression is restricted in the migrating IPs and newborn neurons, but not in RGCs. Moreover, sorted Mib1$^+$ IPs and neurons can send the Notch signal to neighboring cells. Our results reveal that not only newborn neurons but also IPs are essential Notch-ligand-presenting cells for maintaining RGC stemness during both symmetric and asymmetric divisions.

INTRODUCTION

Notch signaling has been proposed to be a key regulator of the orderly progression of cell types during forebrain development (Justice and Jan, 2002). Several studies by genetic fate mapping and time-lapse imaging suggested that RGCs serve as neural stem cells in the developing brain (Anthony et al., 2004; Malatesta et al., 2003; Miyata et al., 2001; Noctor et al., 2001, 2004). Notch signaling promotes the radial glial identity during embryogenesis (Gaiano et al., 2000), and the brain lipid-binding protein (BLBP), a marker of radial glia, is reportedly a direct target of the Notch signaling pathway (Anthony et al., 2005). Therefore, it is clear that RGCs receive Notch signaling during mammalian neurogenesis. However, what type of cells are a relevant cellular source of Notch ligands and how the Notch-Notch ligand interactions are regulated in the repetitive divisions of RGCs are poorly understood, although numerous analyses of Notch-related mutants have been reported (Yoon and Gaiano, 2005).

During asymmetrical division in *Drosophila*, two daughter cells that are initially equivalent choose different fates, a phenomenon mediated by intrinsic and extrinsic factors. In *Drosophila* CNS and sensory organ development, Numb and Neuralized (Neur) are unequally segregated to one sibling cell during asymmetric division, and they determine the fate of the daughter cells by modulating Notch signaling (Le Borgne and Schweisguth, 2003; Rhyu et al., 1994; Spana and Doe, 1996). In those cases, Notch and Delta are already expressed in progenitor cells before asymmetric division, and the Notch modulators, Numb and Neur, ensure that Notch signaling is only activated in one of the sibling cells (Bardin et al., 2004; Le Borgne and Schweisguth, 2003). Thus, the unequal segregation of the Notch modulators and the consequential Notch signaling are critical for the initial binary cell fate determination in *Drosophila*.

In the mammalian telencephalon, however, the *dll1* and *dll3* transcripts are expressed in the postmitotic neurons migrating to the cortical plate, but not in the dividing RGCs at the ventricular surface (VS) (Campos et al., 2001), suggesting that the interaction between the Notch ligands and receptors may not occur between two uncommitted sibling cells during or immediately after their birth at the VS. Instead, Notch signaling may be generated by the interaction between the migrating committed neuronal daughters (IPs and neurons) and the RGCs after the cell fate decision. Although Notch-related genes are well conserved from *Drosophila to* mammals, the Notch activation mechanism in mammalian cortical neurogenesis appears to be different from that in the binary cell fate decision in *Drosophila.*

Recently, it was known that IPs, a type of neurogenic transient amplifying cells, exist between RGCs and newborn neurons in mammalian neurogenesis (Englund et al., 2005; Guillemot, 2005). However, how IPs are implicated in the Notch-Notch ligand interaction has never been considered. Moreover, both sibling cells can adopt the RGC fate in symmetric proliferative division (Guillemot, 2005; Huttner and Kosodo, 2005). Because RGCs do not express the Notch ligands (Campos et al., 2001), they could not send a Notch signal to each other. Therefore, a "third cell" has to send the Notch signal to the two equivalent sibling cells to maintain their stemness. However, the identity of

the third cell needs to be determined. Therefore, the identity of the Notch-ligand-presenting cells sending the Notch signal to the dividing RGCs needs to be clarified, based on recent progress.

Two structurally distinct RING-type E3 ubiquitin ligases, Neur and Mind bomb (Mib), modulate Delta endocytosis in a ubiquitination-dependent manner in the signal-sending cells, to promote Notch activation in the signal-receiving cells (Itoh et al., 2003; Koo et al., 2005; Pavlopoulos et al., 2001). However, the disruption of the *neur1* (Ruan et al., 2001; Vollrath et al., 2001), *neur2*, and *neur1/2* genes (Koo et al., 2007) in mice did not generate the characteristic Notch phenotypes found in the *Drosophila neur* mutants, suggesting that the *neur* homologs are not necessary for cell fate determination in mammalian neurogenesis, in spite of their well-characterized role in *Drosophila*. In contrast, Mib1 regulates the endocytosis of all of the canonical Notch ligands (Deltalike 1, −3, and −4; Jagged 1 and −2), and its disruption in mice exhibits pan-Notch defects (Koo et al., 2005). Because Mib1 functions in the signal-sending cells and is required for both the Deltalike- and Jagged-mediated Notch signaling in mammalian development (Koo et al., 2007), the genetic mutant of Mib1 would be an excellent model to elucidate the identity of the signal-sending cells and the action mode of Notch signaling.

Therefore, we have generated conditional mutants that disrupt the *mib1* gene in the developing telencephalon. These mutant mice display complete abrogation of Notch activation, defective RGC maintenance, and premature differentiation to intermediate progenitors (IPs) and finally neurons. These phenotypes were completely rescued by the introduction of active Notch1, demonstrating that the neurogenic phenotypes in the Mib1 mutant mice are caused by defective Notch activation. The monitoring of RGC divisions using the DiI labeling method (Imai et al., 2006; Miyata et al., 2001, 2004) revealed that Mib1 mutant RGCs exhibited the symmetric divisions that produce either two IPs or two neurons. Using several independent methods, we identified not only young neurons but also IPs as Mib1-expressing cells. A FACS-based functional analysis further revealed that Mib1$^+$ cortical cells display only limited neurosphere-forming activity and efficiently trigger Notch signaling in the neighboring cells. Furthermore, retroviral-mediated gene manipulation at the single-cell level showed that Notch signaling in the RGCs is activated by Mib1-expressing IPs produced by neighboring RGCs. These results demonstrate the role of Mib1-expressing IPs as an important cellular source of the Notch signal that maintains the self-renewal of RGCs together with newborn neurons and provide a mechanism for the RGC self-renewal and for expanding the RGC pool in mammalian neurogenesis.

RESULTS

Conditional Inactivation of Mib1 in the Nervous System

To inactivate *mib1* in neural precursor cells, we crossed *mib1$^{f/f}$* mice, in which exons 2 and 3 of the *mib1* gene are flanked by loxP sites (Koo et al., 2007), with a transgenic mouse line that expresses Cre recombinase under the control of the *nestin* promoter (Graus-Porta et al., 2001; Tronche et al., 1999). To test the deletion efficiency of the *mib1* gene in the *Nestin-cre;mib1$^{f/f}$* forebrain, quantitative RT-PCR, in situ hybridization, and immunoblotting were carried out at different stages. The *mib1* transcripts were readily observed in both the wild-type and mutant forebrains at embryonic day (E) 11.5 (data not shown) but were almost undetectable in the mutants at E13.5 (see Figures S1A and S1B available online). Consistently, the Mib1 protein expression was greatly reduced in the mutant forebrain at E13.5, while its expression was relatively intact at E12.5 (Figure S1C).

The *Nestin-cre;mib1$^{f/f}$* mice were embryonic lethal around E18.5. While the mutant forebrains showed relatively intact integrity and structure at E12.5 (Figures 1A and 1B), the brain structure was severely disorganized. The lateral ventricles were enlarged, and the ganglionic eminence was disintegrated at E14.5 (Figures 1C and 1D). The ventricular walls in the wild-type forebrains showed well-polarized cells, with the eosinophilic apical membrane domain facing the lumen (Figures 1E and 1G, arrowheads). In contrast, the apical membrane domain was completely lost (Figures 1F and 1H), and the aberrant fibrous reticulum emerged at the ventricular surface (VS) of the dorsal neocortex in the mutant forebrains (Figure 1F, arrow). Cells adjacent to the VS lost their polarity, and some of the cells protruded into the ventricle of the mutant forebrains (Figure 1H, arrows). These results indicate that Mib1 is critical for the integrity of the forebrain structure.

Depletion of RGCs in the *Nestin-cre;mib1$^{f/f}$* Forebrains

Because the integrity was severely disrupted in the *Nestin-cre;mib1$^{f/f}$* forebrains, we first examined the status of the RGCs. At E12.5, the Nestin$^+$ neural progenitors were properly located and showed no morphological difference between the wild-type and mutant forebrains (Figures 2A and 2B). At E14.5, however, the number of Nestin$^+$ cells was greatly reduced in the mutant forebrains (Figures 2C and 2D). BrdU labeling experiments revealed the progressive decrease of S-phase cells in the mutant forebrains (Figures S2A–S2C). In addition, *pax6*, a transcriptional factor expressed in dorsal neural progenitor cells, was remarkably decreased in the E14.0 mutant brains (Figures 2E and 2F), indicating that RGCs are depleted in the absence of Mib1.

To assess the integrity of the RGCs, we examined the expression of an RGC marker, RC2 (Hartfuss et al., 2001). The RC2 immunoreactivity was grossly similar between the neocortexes of the wild-type and mutant mice at E13.5 (Figures 2I and 2J). A closer examination, however, revealed that the RGCs in the marginal zone and in the vicinity of the VS were undergoing regression of their processes and were losing their connection with the pial and the VS in the mutant neocortexes (Figures 2L, 2M, 2O, and 2P). At E14.0, the number of RC2-expressing cells was dramatically decreased in the marginal zone and the VS. Moreover, their polarity was disorganized, and the morphology of each cell was shriveled (Figures 2K, 2N, and 2Q). The apical endfeet of RGCs are known to be tightly associated with the adherens junctional complex at the VS (Cappello et al., 2006; Imai et al., 2006). Immunostaining of ZO-2 (Itoh et al., 1999; Jesaitis and Goodenough, 1994), one of the core components in this adherens junction between the RGCs (Aaku-Saraste et al., 1996), revealed the loss of the adherens junction in the mutant forebrains at E14.0 (Figures S3A and S3B). At E14.5, RC2 expression

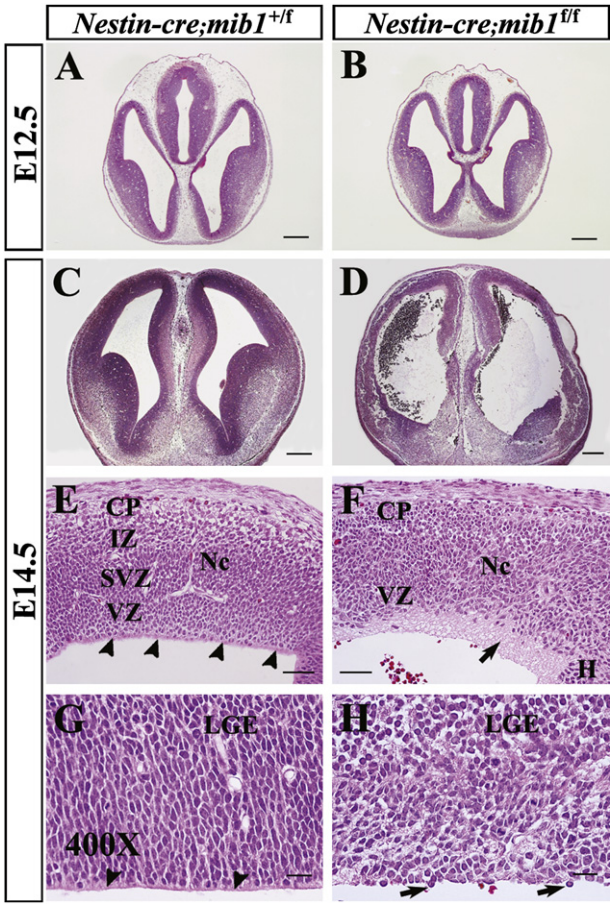

Figure 1. Disorganization of the Neocortex and Subcortical Regions in the *Nestin-cre;mib1*$^{f/f}$ Forebrain

(A–H) H&E staining of paraffin-embedded coronal sections of the wild-type (A, C, E, and G) and *Nestin-cre;mib1*$^{f/f}$ (B, D, F, and H) forebrains. (E and F) The dorsal neocortex. (G and H) The ventricular wall of the lateral ganglionic eminence. The width of the neocortexes in the *Nestin-cre;mib1*$^{f/f}$ forebrains was much thinner than that in the wild-type. The ventricular zones of the wild-type mice had a dense composition filled with the nuclei of progenitor cells, but not in the *Nestin-cre;mib1*$^{f/f}$ mice. Arrowheads in (E) and (G) show the eosinophilic apical membrane domain in the wild-type forebrain. The arrow in (F) indicates the aberrant fibrous reticulum in the *Nestin-cre;mib1*$^{f/f}$ mice. Arrows in (H) represent aberrant protruding cells in the ventricular surface of the mutant brains. Nc, neocortex; H, hippocampal neuroepithelium; LGE, lateral ganglionic eminence; CP, cortical plate; IZ, intermediate zone; SVZ, subventricular zone; VZ, ventricular zone. Scale bars: 200 μm in (A)–(D), 50 μm in (E) and (F), 20 μm in (G) and (H).

was completely lost in the mutant forebrains (data not shown), indicating that the RGCs lose their integrity progressively in the absence of Mib1.

To test whether the depletion of RGCs is due to defective Notch activation, we examined the expression of Notch target genes. As expected, the expression levels of the *hes1*, *hes5*, and *blbp* transcripts were dramatically decreased in the mutant brains, as compared to the wild-type brains (Figures 2G and 2H and Figure S1A). These results suggest that the *mib1* disruption inhibits Notch signaling, which depletes the RGCs gradually. To examine whether the depletion of the RGCs in the mutant brains is coupled with increased cell death, TUNEL staining of the forebrain sections was performed. There were no remarkable differences between the wild-type and mutant brains at E14.5 (Figure S4), indicating that apoptotic cell death is not the cause of the loss of RGCs in the mutant brains.

Premature Neuronal Differentiation in the *Nestin-cre;mib1*$^{f/f}$ Forebrains

Neurons can be generated directly and indirectly, by the asymmetric division of RGCs (direct neurogenesis) at the VS and via the symmetric division of IPs in the basal region (indirect neurogenesis), respectively (Englund et al., 2005; Guillemot, 2005). However, there is no report on how indirect neurogenesis is affected by loss of Notch signaling, although premature neuronal differentiation has been reported by numerous analyses of Notch-related mutants (Yoon and Gaiano, 2005). Therefore, we examined whether the premature depletion of RGCs in the mutant brains is due to uncontrolled direct or indirect neurogenesis. Immunostaining for β-tubulin III (data not shown) and Tbr1 (Figures 3A and 3B), postmitotic neuronal markers (Englund et al., 2005), did not reveal a significant difference between the wild-type and mutant neocortexes at E13.5. Intriguingly, the β-tubulin III$^+$ neurons emerged in the VS of the mutant neocortexes at E13.75 (Figures 3H and 3h, an arrow). Considering the fact that the IPs revealed by the Tbr2 immunostaining (Englund et al., 2005) were not observed in the vicinity of these ectopic β-tubulin III$^+$ neurons at E13.75 (Figure S5), they might be prematurely generated by the direct neurogenesis occurring in the VS.

Concomitantly, the Tbr2$^+$ IPs were dramatically increased in the VZ of the mutant neocortexes at E13.5, when the increase of postmitotic neurons was not evident yet (Figures 3D and 3d). At E14.0, most of the cells in the mutant neocortexes had differentiated into β-tubulin III$^+$ neurons, except in several subventricular regions (Figure 3J, arrow). The residual cells in the β-tubulin III$^-$ subventricular regions were Tbr2$^+$ (Figure 3L, an arrow). In the Tbr2$^+$ regions of the mutant neocortexes at E13.5 and E14.0, basal mitoses that had not occurred at the VS (NS-Div) (Miyata et al., 2004) were dramatically increased at the expense of mitosis at the VS (S-Div) (Figures 3E, 3F, 3M, and 3N and Figures S2D–S2G). In the hippocampal neuroepithelium of the mutant mice, the premature differentiation was delayed, as compared to the neocortex (Figures 3J, 3L, and 3N, arrowheads), which might be due to the delayed deletion of the *mib1* gene (Figure S1B, arrow). The Tbr2$^+$ IPs were sequentially decreased (Figure 3P) and finally converted to β-tubulin III$^+$ neurons at E14.5 (Figure 3R). These results suggest that the disruption of the *mib1* gene leads to the premature differentiation of RGCs to IPs, which eventually differentiate to postmitotic neurons in the VZ (Figure 3R). Collectively, the depletion of RGCs in the mutant forebrains might be due to the premature differentiation of RGCs, to either β-tubulin III$^+$ postmitotic neurons at the VS (accelerated direct neurogenesis) or to IPs that eventually differentiate into postmitotic neurons (accelerated indirect neurogenesis).

To confirm that the premature differentiation of RGCs to IPs and neurons is due to the inactivation of *mib1*, we analyzed another type of *mib1* conditional knockout mice induced by the *hGFAP* promoter (Zhuo et al., 2001) (*hGFAP-cre;mib1*$^{f/f}$ mice).

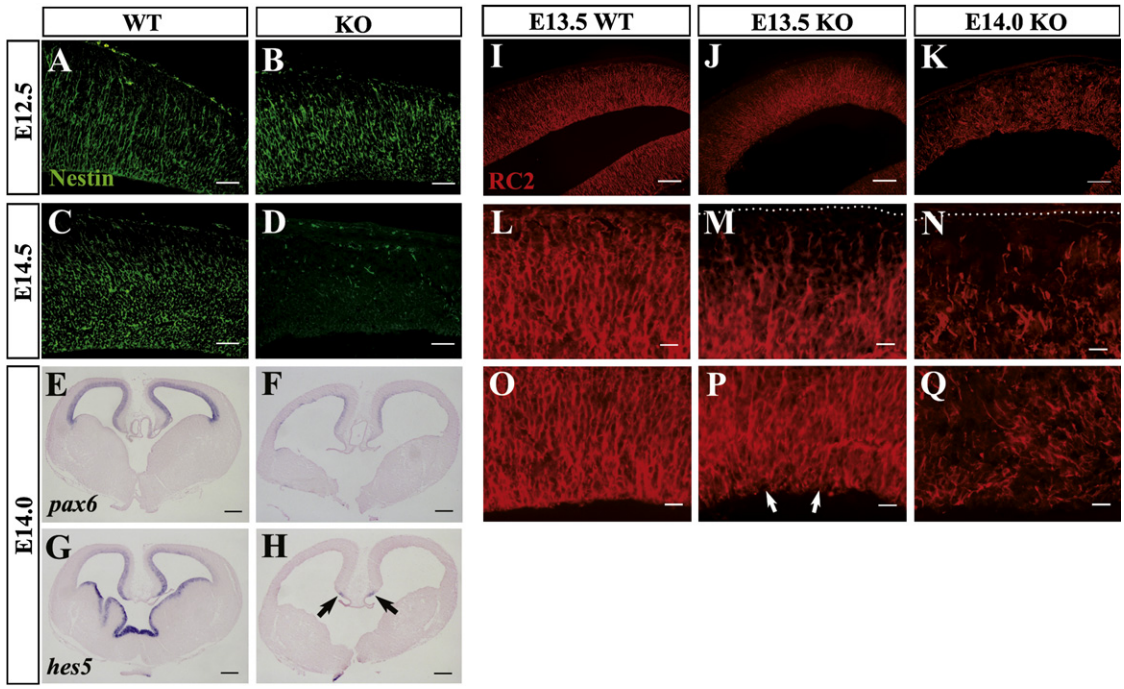

Figure 2. Progressive Degeneration of RGCs in the *Nestin-cre;mib1*$^{f/f}$ Brains after the Ablation of *mib1*

(A–D) The expression of Nestin in the E12.5 (A and B) and E14.5 (C and D) neocortexes from the wild-type (A and C) and *Nestin-cre;mib1*$^{f/f}$ (B and D) embryos. (E–H) In situ hybridization of *pax6* (E and F) and *hes5* (G and H) on the frozen sections of the E14.0 wild-type (E and G) and *Nestin-cre;mib1*$^{f/f}$ (F and H) forebrains. Note the residual *hes5* transcripts (arrows in [H]) in the hippocampal neuroepithelium, where the *mib1* mRNA still exists at this stage.

(I–Q) The expression of RC2. Note the progressive regression of the radial glial fiber in the neocortex of the *Nestin-cre;mib1*$^{f/f}$ mice. (L–N) Higher-magnification images of the basal endfeet of RGCs at the pial surface. Dotted lines in (M) and (N) represent the pial surface. (O–Q) Higher-magnification images of the apical endfeet of RGCs at the ventricular surface. Arrows in (P) represent decreased RC2 expression at the ventricular surface. Scale bars: 200 μm in (E)–(H), 100 μm in (I)–(K), 50 μm in (A)–(D), 20 μm in (L)–(Q).

These mutant mice also showed similar phenotypes to the *Nestin-cre;mib1*$^{f/f}$ mice during midneurogenesis (Figure S6), although the phenotypic change was delayed in the ventral neocortex, which might be due to a distinct pattern of Cre-mediated recombination, from the hippocampal neuroepithelium to the ventral neocortex (from the medial to lateral direction) (data not shown) (Figure S6J, arrow). Because the deletion of the *mib1* gene by the two different promoters, *hGFAP* and *Nestin*, leads to the exact phenocopy, premature differentiation of RGCs to IPs and neurons must be caused by the inactivation of *mib1*.

To examine whether Notch signaling regulates the differentiation of RGCs to IPs in indirect neurogenesis, we analyzed the *hGFAP-cre;Rosa-Notch1* mice (Murtaugh et al., 2003), in which Notch signaling is constitutively activated in RGCs by Cre recombinase. As expected, the Tbr2^{+} IPs and the NS-Div were greatly reduced in the *hGFAP-cre;Rosa-Notch1* neocortexes (Figures S7A–S7D). Therefore, the fate of the IP is inhibited by active Notch signaling, which is consistent with the transient increase of IPs in the *Nestin-cre;mib1*$^{f/f}$ and *hGFAP-Cre;mib1*$^{f/f}$ forebrains.

Because Mib1 interacts with another substrate, DAPK (Jin et al., 2002), we examined whether the phenotypic changes in the *Nestin-cre;mib1*$^{f/f}$ mice are entirely caused by the defective Notch signaling. We bred the *Nestin-cre;mib1*$^{f/f}$ mice with the *Rosa-Notch1* mice (Murtaugh et al., 2003). As expected, the premature differentiation of RGCs in the *Nestin-cre;mib1*$^{f/f}$ forebrains was completely inhibited by the activation of Notch1 (Figure S8). These results show that the premature differentiation of RGCs in the inactivation of the *mib1* gene is due to the defective Notch signaling.

Direct Monitoring Revealed Non-Stem-like Behaviors of RGCs in *mib1* Null Cortical Slices

To better explain the aforementioned in vivo phenotypes of the mutant forebrains, we sought to directly monitor the behavior of the RGCs and their daughter cells. Cerebral hemispheres prepared from the wild-type and *hGFAP-cre; mib1*$^{f/f}$ mice at E13.5 were labeled with DiI and sliced (Imai et al., 2006; Miyata et al., 2001, 2004). In the wild-type slices, the RGCs frequently generated daughter cells that subsequently divided at the VS (Figures 4A and 4B). This exhibition of two rounds of division at the surface is typical in the cerebral walls at this and similar ages (Miyata et al., 2004; Noctor et al., 2004), as it contributes to the maintenance of the progenitor pool. As reported in several previous studies (Miyata et al., 2004; Noctor et al., 2004), wild-type RGCs showed generally two different types of division patterns, symmetric proliferative division (6 of 28 cases observed) and asymmetric IP- or neuron-generating division (22 of 28 cases observed) (Figures 4A, 4B, and 4U).

In striking contrast, however, the mutant slices showed the following two patterns that were strongly biased to the neuronal

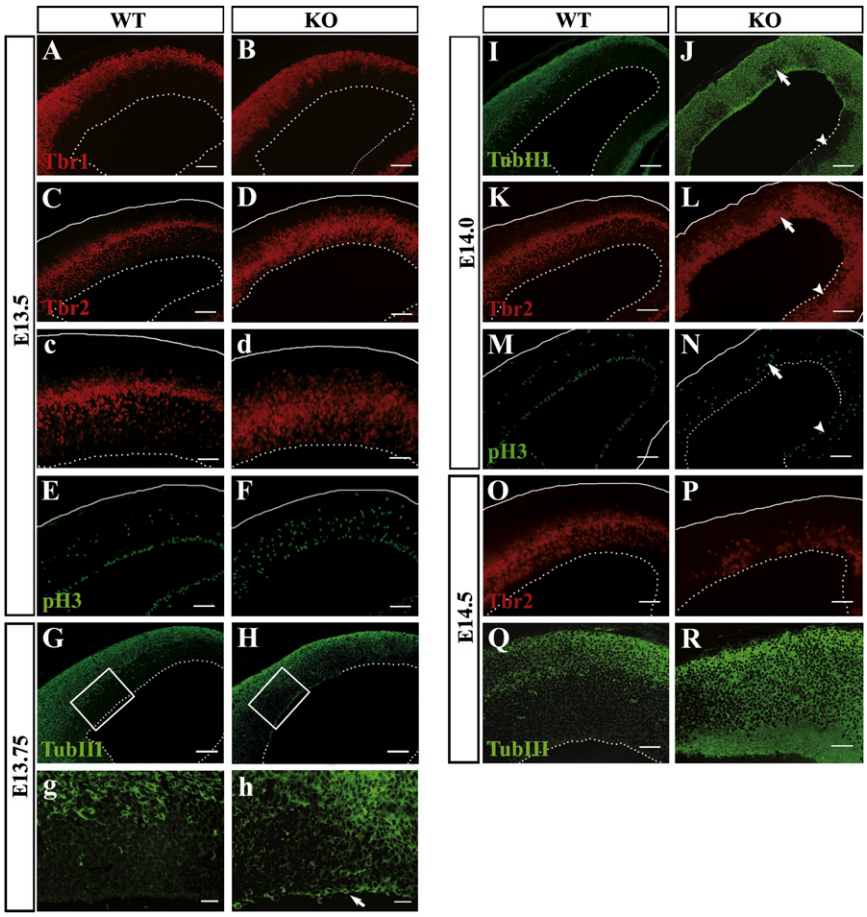

Figure 3. Premature Neuronal Differentiation in the *Nestin-cre;mib1*$^{f/f}$ Forebrains

(A and B) Tbr1$^+$ preplate neurons in the wild-type (A) and *Nestin-cre;mib1*$^{f/f}$ (B) forebrains at E13.5.

(C, D, c, d, K, L, O, and P) Tbr2$^+$ intermediate progenitors in the wild-type and *Nestin-cre;mib1*$^{f/f}$ mice. Panels (c) and (d) show higher magnification images of (C) and (D), respectively.

(E, F, M, and N) Mitotic cells labeled by anti-phospho-histone H3 antibody. Labeled cells at the ventricular surface represent S-Div, and the others represent NS-Div.

(G, H, g, h, I, J, Q, and R) β-tubulin III staining of the wild-type and *Nestin-cre;mib1*$^{f/f}$ mice. Panels (g) and (h) show higher-magnification images of the boxed regions in (G) and (H), respectively. The arrow in (h) indicates the accumulation of differentiated neurons at the ventricular surface. The sections of (I), (K), and (M) and (J), (L), and (N) are all adjacent, respectively. Note that the β-tubulin III$^-$ regions are Tbr2$^+$ and mitotic in the *Nestin-cre;mib1*$^{f/f}$ brains (arrows in [J], [L], and [N]). Arrowheads in (J), (L), and (N) represent the region that shows delayed phenotypes in the hippocampal neuroepithelium. The solid lines represent the pial surface, and the dotted lines represent the ventricular surface. Scale bars: 100 μm in (A)–(P); 50 μm in (c), (d), (Q), and (R); 20 μm in (g) and (h).

lineage, at the expense of the apically connected, undifferentiated progenitor cells. Type I (9 of 51 cases observed). As exemplified in Figure 4C, the RGCs, which appeared to have lost the basal process as observed in vivo (Figures 2M and 2N), divided at the VS, and their daughter cells became neurons that were β-tubulin III$^+$ (Figures 4D–4H). The daughter neurons pair-generated from this type of mitosis (symmetric terminal) at the VS remained in the VZ without further migration toward the CP, consistent with our observation in vivo that ectopic neuronal zones were formed along the VS (Figures 3H and 3h). Type II (42 out of 51 cases). Two daughter cells were generated at the VS, and they soon lost their apical attachment and migrated together to the subventricular zone (SVZ). Some of the basally migrating daughter cells divided at the SVZ (Figure 4I, blue arrowheads). Figure 4J shows a case in which two daughter cells (Figure 4J, yellow arrowhead) divided at the SVZ to generate four granddaughter cells (Figure 4J, blue arrowheads). These granddaughter cells were all identified to be neurons that were β-tubulin III$^+$ and Tbr2$^+$ (Figures 4K–4T). In this type, even though the division of the founder RGCs could lead to the formation of three- or four-cell clones, all of the clones were formed in the SVZ and appeared to consist purely of neurons. Therefore, the mitotic daughter cells generated from the founder RGCs in the mutant slices were considered to be IPs, which are known to be Tbr2$^+$, rather than undifferentiated progenitors (RGCs), which are generally RC2$^+$. The loss of RC2 expression at the VS, the increase of Tbr2$^+$ IPs, and the resultant premature neuronal differentiation shown in the fixed mutant brain (Figures 2P and 3) can be explained by these abnormally frequent divisions committed to the neuronal lineage.

In addition to the mutant neocortex, we also observed the same phenotypes in brain slices treated with DAPT, a γ-secretase inhibitor. The decreased expression of the Notch target genes, *hes1* and *hes5*, by the DAPT treatment indicates that Notch signaling was efficiently inhibited (Figure S9A). As shown in the *mib1*-null forebrains (Figure 3), Tbr2$^+$ cells were dramatically increased in the basal region of the VZ, while β-tubulin III$^+$ cells emerged in the VS by the DAPT treatment (Figure S9B). Interestingly, the clonal tracing experiments revealed that the RGCs showed the type I (9 of 21 cases observed) and type II (12 of 21 cases observed) behaviors, as described above. These distinct patterns of RGC behavior did not appear to depend on the cell cycle status of the RGCs, because the RGCs in both the G1-S and G2-M phases at the initiation of the DAPT treatment exhibited both the type I and II patterns (Figure S9C).

The symmetric proliferative division, which increases the progenitor pool by making two RGCs at the VS (Guillemot, 2005; Miyata et al., 2004), was not detected at all in the slice culture experiments with the mutant forebrains. Taken together, the time-lapse analysis clearly demonstrated that the RGCs in the *mib1* conditional knockout brains cannot undergo divisions to maintain or increase the number of RGCs, and they instead undergo the symmetric divisions that generate two daughters belonging

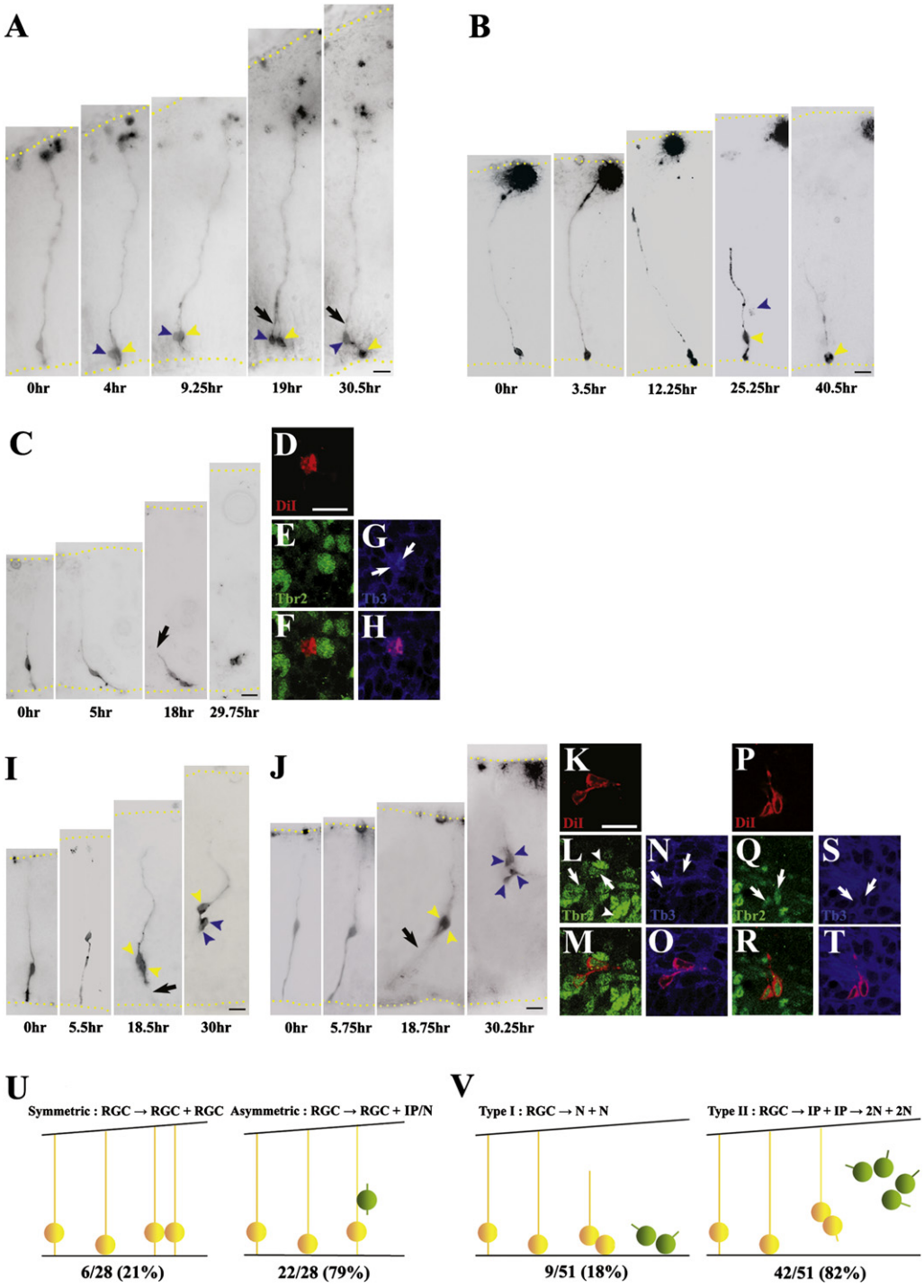

Figure 4. An RGC Cannot Maintain Another RGC in the Next Round of Division in *hGFAP-cre;mib1*$^{f/f}$ Mice

(A) A typical symmetric proliferative division, which generates two RGCs after S-Div in the wild-type slice at E13.5. After dividing at the ventricular surface, a bipolar RGC generated two RGCs. One of them divided again at the ventricular surface after 30.5 hr of tracing (yellow arrowhead), and the other one maintained its basal process (arrow) and remained in the VZ instead of migrating to the CP (blue arrowhead), which are typical characteristics of symmetric proliferative division.

(B) A typical asymmetric division, which generates another RGC after S-Div in the wild-type slice at E13.5. A bipolar RGC divided at the ventricular surface. It generated an RGC, which can continue S-Div sequentially (yellow arrowhead), and a neuronal daughter, which can migrate to the cortical plate (blue arrowhead). The neuronal daughter was out of focus after 40.5 hr of tracing.

(C–H) Type I division. A bipolar RGC divided at the ventricular surface and lost its basal processes (arrow). After the tracing, the slice was fixed and subjected to Tbr2 and β-tubulin III staining. Panel (D) shows DiI-labeled daughter cells, and panels (F) and (H) are merged images. The resultant two daughter cells are Tbr2^{-}

to the neuronal lineage (type I, N-N division; type II, IP-IP division; summarized in Figure 4V).

Transient *mib1* Expression during the Neuronal Differentiation

To clarify the role of Mib1 in the maintenance of RGCs and the proper neuronal differentiation in the developing brain, we examined the types of cells expressing Mib1. We used *mib1* knockout mice, which contain a LacZ reporter transgene in the *mib1* genomic locus (Koo et al., 2005). X-gal staining of the $mib1^{+/LacZ}$ forebrain revealed that the β-galactosidase activity was specifically detected in the SVZ and the intermediate zone (IZ), but rarely in the VZ and the CP (Figure 5A). Costaining with β-tubulin III, Tbr2, and MAP2 (mature neurons in the CP) revealed β-galactosidase activity in the β-tubulin III^+ neurons (Figures 5B and 5b) and the $Tbr2^+$ IPs (Figures 5C and 5c, arrows) between the IZ and the basal side of the SVZ. Although the β-galactosidase activity cannot completely represent the behavior of the Mib1 protein, because of its different stability and turnover, it is clear that Mib1 is expressed at a specific stage during neuronal differentiation from RGCs to early-born neurons and is "turned-off" during neuron maturation.

To identify the specific cells expressing Mib1, fluorescence double in situ hybridization was carried out. The *mib1* transcripts were localized in the VZ and the SVZ, but not in the VS of the neocortex (Figure 5F). A more detailed view revealed that almost all of the $tbr2^+$ cells and $dll1^+$ cells expressed *mib1* (Figures 5H–5M), indicating that the *mib1* transcripts were detected in the early migratory state of IPs or newborn neurons after the cell fate determination at the VS. Because it was not clear which Notch ligands are expressed in IPs, we conducted double in situ hybridization and found that $tbr2^+$ IPs readily expressed *dll1* or *dll3* (Figure S10). To further examine whether Mib1 is expressed in the IPs and postmitotic neurons, we isolated neural stem cells, IPs, and neurons from the transgenic Notch reporter (TNR) neocortex, using the neural progenitor marker CD133 and the EGFP signal (Mizutani et al., 2007) (Figure 6A). The $CD133^-$ and $CD133^+/EGFP^{lo/-}$ populations highly expressed β-tubulin III and Tbr2, respectively, indicating that they contain postmitotic neurons and IPs, respectively. In contrast, the $CD133^+/EGFP^{hi}$ populations highly expressed Nestin, but not β-tubulin III and Tbr2, indicating that they contain the RGCs. As expected, Mib1 was highly expressed in the $CD133^-$ and $CD133^+/EGFP^{lo/-}$ populations, but not in the $CD133^+/EGFP^{hi}$ populations (Figure 6B). Because Mib1 is essential for generating functional Notch ligands (Koo et al., 2005), these results suggest that $Tbr2^+$ IPs and postmitotic neurons might be the responsible Notch-signal-sending cells.

Freshly Harvested Mib1-Expressing Cells Generate Efficient Notch Signaling

Can Mib1-expressing cells trigger Notch signaling in the surrounding cells? To answer this question, we used C2C12 cells expressing Notch1 (N1-C2C12) to evaluate the Notch activity after coculture with the sorted cells (Koo et al., 2005; Lindsell et al., 1995). For the quantification of the Notch signaling activity, the N1-C2C12 cells were transfected with the Hes1-luc or Hes1-△ABluc construct (Jarriault et al., 1998) prior to coculture with the sorted cortical cells. As expected, while $CD133^+/EGFP^{hi}$ cells did not trigger a Notch signal in the surrounding C2C12 cells, Notch-signal-sending activity was readily detected in the Mib1-expressing $CD133^+/EGFP^{lo/-}$ and $CD133^-$ cells (Figure 6C).

To further address the above issue, we stained the cortical cells from the E13.5 $mib1^{+/LacZ}$ brains using a vital fluorogenic β-gal substrate, fluorescein digalactopyranoside (FDG), and sorted the β-gal^+ and β-gal^- cells by flow cytometry (Figure 6D). When the β-gal^+ and β-gal^- cells were cultivated in the neurosphere culture media with EGF and bFGF for 7 days, the neurosphere-forming activity of the β-gal^+ cells was much lower than that of the β-gal^- cells (Figure 6E), confirming that the β-gal^+ cells were mostly non-RGCs belonging to the neuronal lineage. Moreover, the β-gal^+ cells efficiently stimulated Hes1-luc, ~1.8-fold more than the β-gal^- cortical cells (Figure 6F). The decreased activity of β-gal^+ sorted cells compared to nonsorted wild-type cells might be due to tough procedures and time-delaying by the sorting events. Collectively, these results suggest that the Mib1-expressing IPs and postmitotic neurons efficiently generate Notch signaling to the neighboring cells, possibly RGCs.

Notch Activation in RGCs by the Mib1-Expressing IPs and Postmitotic Neurons Produced by Neighboring RGCs

Neuronal daughters migrate along the radial process of the parent RGCs during the initial phase of their migration (Noctor et al., 2004) and also through the enriched somata of the neighboring RGCs (Miyata, 2007). Thus, RGCs can interact with $Mib1^+$ IPs

(E and F), β-tubulin III^+ (G and H), showing that type I division is symmetric terminal division generating two neurons. Arrows in (G) represent β-tubulin III^+ DiI-labeled daughter cells.

(I–T) Type II division. A bipolar RGC divided into two daughter cells, which migrated to the SVZ ([I and J], yellow arrowheads). The apical processes of the parental RGC were lost after the divisions ([I and J], arrows). Panel (I) shows one of the daughter cells that divided into two granddaughter cells (blue arrowhead). In (J), two daughter cells divided into four granddaughter cells after the 30.25 hr tracing (blue arrowheads). Panels (K) and (P) show DiI-labeled granddaughter cells, and (M), (O), (R), and (T) are merged images. The resultant four granddaughter cells have low Tbr2 expression (arrows in [L] and [Q]), suggesting that these cells originated from IPs highly expressing Tbr2. The cells indicated by arrowheads in (L) have high Tbr2 expression and seem to be the IPs before NS-Div. The resultant four granddaughter cells are all β-tubulin III^+ neurons ([N, O, S, and T], arrows), showing that type II division is two sequential symmetric divisions generating four neurons through two IPs. The yellow dotted lines represent the ventricular surface and the pial surface. Scale bars: 20 μm in (A)–(T).

(U) Schematic illustration of normal RGC divisions in the wild-type slices. In the wild-type slices, an RGC shows two different types of divisions, symmetric proliferative division and asymmetric division. In asymmetric division, a RGC generates a neuronal daughter cell (an IP or a neuron, represented as a green shape), which initially migrates to the SVZ. The frequency of each type of division is indicated on the figure.

(V) Schematic illustration of aberrant divisions in the mutant slices. In type I division, a bipolar RGC generates two neurons in the vicinity of the ventricular surface. In type II division, a bipolar RGC generates four neurons in the SVZ through two IPs. The green shapes represent neurons. The frequency of each type of division is indicated on the figure.

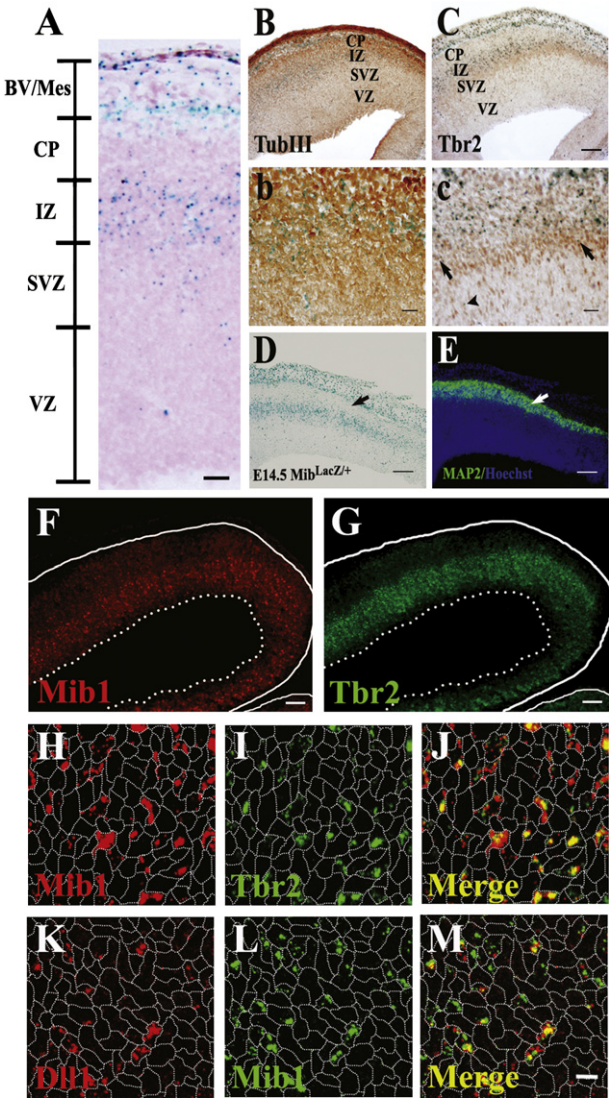

Figure 5. Restricted Expression of *mib1* in IPs and Neurons during the Radial Migration

(A) X-gal-stained section of the E13.5 *mib1*$^{+/LacZ}$ brain. The β-galactosidase activity is detected mainly in the IZ and the SVZ. The extracerebral mesenchymal tissue and the vasculatures also have β-galactosidase activity. There is little β-galactosidase activity in the cortical plate and the VZ.

(B and b) β-tubulin III staining on an X-gal-stained section of the E13.5 *mib1*$^{+/LacZ}$ brain. Panel (b) shows higher-magnification images of (B).

(C and c) Tbr2 staining of an X-gal-stained section of the E13.5 *mib1*$^{+/LacZ}$ brain. Panel (c) shows higher-magnification images of (C). Arrows in (c) indicate Tbr2^{+} X-gal-stained cells. The arrowhead in (c) indicates an X-gal-stained migratory Tbr2^{+} progenitor from the apical side.

(D and E) X-gal staining of a section of the E14.5 *mib1*$^{+/LacZ}$ brain (D) costained with the neuronal marker MAP2 (in green) and Hoechst (in blue) on the same section (E). Arrows in (D) and (E) indicate the same region in the MAP2^{+} neuronal layer of the section.

(F–M) Fluorescence double in situ hybridization reveals *mib1* expression in *tbr2*$^{+}$ or *dll1*$^{+}$ cells. Images were obtained by confocal microscopy. (F), (G), (H), (I), and (J) are *mib1* (in red) and *tbr2* (in green) transcripts in the neocortex of the E14.0 wild-type brain. (K), (L), and (M) are *mib1* (in green) and *dll1* (in red) transcripts in the neocortex of the E14.0 wild-type brain. (H–M) show amplified images in the SVZ/VZ border of the stained neocortexes. (J) and (M) are merged images of each experiment. In (F) and (G), the solid lines represent the pial surface and the dotted lines represent the ventricular surface. The dotted lines in (H), (I), (J), (K), (L), and (M) represent the borderlines between cells, which were identified by DIC images. Scale bars: 100 μm in (B)–(G), 50 μm in (A), 20 μm in (b) and (c), 10 μm in (H)–(M).

and neurons generated from either parent RGC or neighboring RGC, for the activation of Notch signaling (Figure 7A, left panel). In order to examine whether RGCs can interact with the Mib1-expressing IPs and postmitotic neurons generated by neighboring RGCs to get Notch signaling, we applied the Cre-IRES-GFP retrovirus on the *mib1*$^{f/f}$ and the *mib1*$^{+/f}$ brains (Figure 7A, right panel). This retroviral system was validated by using *Rosa26R* reporter mice, in which Cre-mediated genomic recombination in the GFP^{+} cells was confirmed by the expression of LacZ gene from the flanking LacZ cassette (Figure 7B). Because the Cre-IRES-GFP retrovirus worked well, we applied the same virus to E13.5 Rosa-Notch1 embryos, in which the efficient genomic recombination results in the forced expression of Notch1 ICD in the infected cells. As expected, the forced expression of Notch1 ICD inhibited the differentiation of infected GFP^{+} cells (Figures 7C and 7D).

When the same Cre-IRES-GFP retrovirus was applied to E13.5 *mib1*$^{f/f}$ brains, the mitotic and migratory behaviors of the GFP^{+} cells in *mib1*$^{f/f}$ brains were similar to those of the GFP^{+} cells in *mib1*$^{+/f}$ brains. These experimental groups showed almost equivalent percentages of PCNA expression by GFP^{+} cells in the VZ: 36.4% ± 3.9% at 3 days (n = 5) and 30.4% ± 4.2% at 4 days (n = 5) in the *mib1*$^{f/f}$ group and 34.7% ± 2.3% at 3 days (n = 5) and 27.5% ± 4.7% at 4 days (n = 5) in the *mib1*$^{+/f}$ group. The ratios of PCNA^{+} cells among the GFP^{+} cells in the *mib1*$^{f/f}$ and *mib1*$^{+/f}$ brains infected with the Cre retrovirus were much higher than those (11.7% ± 6.3%, n = 5) in the wild-type brains infected with the dominant-negative Mastermind-like (DN-MAML) retrovirus, which blocks the transcriptional activation of Notch ICD (Weng et al., 2003) (Figures 7C and 7D). Furthermore, there was no difference in the number of Tbr2^{+} IPs cells between mib1$^{+/f}$ and mib1$^{f/f}$ brains (Figures 7E and 7F). These results show that RGCs must have executed Notch signaling properly to maintain their stemness, through the interaction with neuronal daughter cells produced by neighboring RGCs, in the absence of the interaction with its own neuronal daughter cells.

DISCUSSION

It is well known that RGCs require Notch signaling to maintain their stemness (Anthony et al., 2005; Gaiano et al., 2000; Yoon et al., 2004). However, the types of cell-cell interactions that allow RGCs to receive Notch signaling were not clear. This study revealed that Mib1-expressing IPs as well as postmitotic neurons are the responsible signal-sending cells, which transduce the Notch signal to RGCs to maintain their capacity for self-renewal. In addition, RGCs can interact with Mib1-expressing IPs as well as postmitotic neurons produced by neighboring RGCs, which make the RGCs also able to maintain their capacity for self-renewal during asymmetric division and to expand their pool by symmetric division in mammalian neurogenesis.

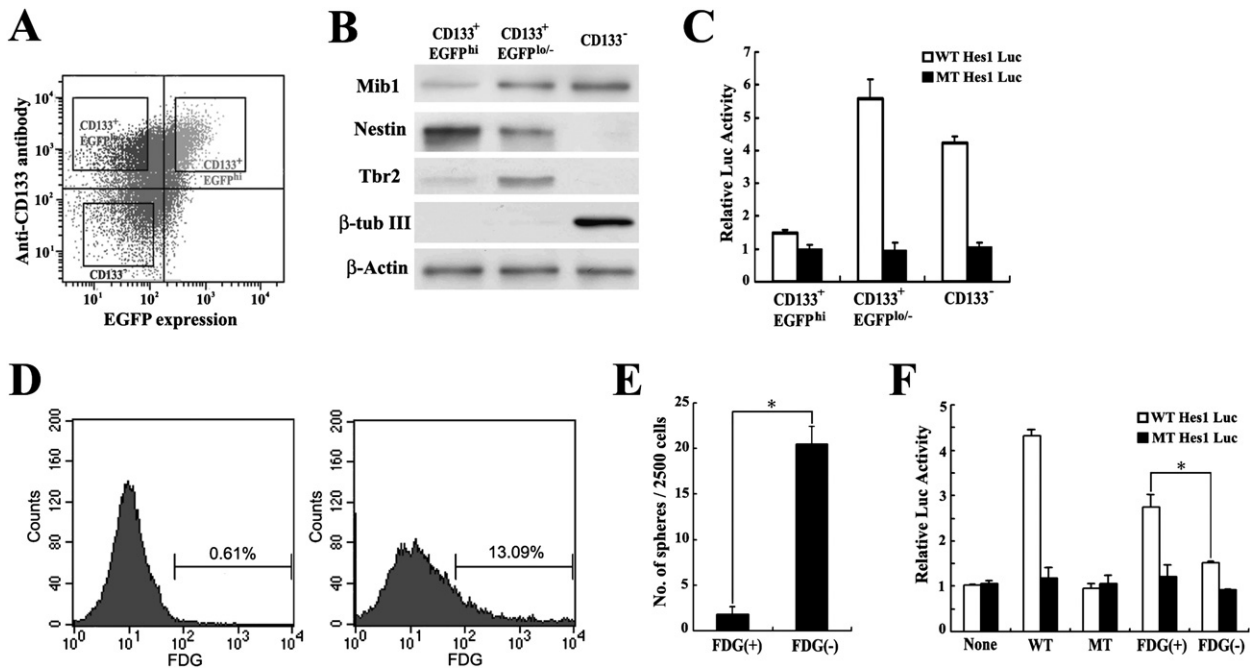

Figure 6. Freshly Harvested Mib1-Expressing Cells Efficiently Generate Notch Signaling

(A) FACS plot of E14.5 TNR neocortical cells.

(B) Freshly isolated CD133$^+$/EGFP^{hi}, CD133$^+$/EGFP$^{lo/-}$, and CD133$^-$ cells were subjected to Western blotting analyses.

(C) CD133$^+$/EGFP$^{lo/-}$ and CD133$^-$ cells, but not CD133$^+$/EGFP^{hi} neural stem cells, were competent to send the Notch signal. CD133$^+$/EGFP^{hi}, CD133$^+$/EGFP$^{lo/-}$, and CD133$^-$ cells were cocultured with N1-C2C12 cells transfected with the wild-type (white bars) and mutant (black bars) Hes1-Luc vectors. Error bars show SD.

(D) Cortical cells from the E13.5 *mib1*$^{+/LacZ}$ brains were sorted by flow cytometry after staining with the vital fluorogenic β-gal substrate, fluorescein digalactopyranoside (FDG).

(E) The number of neurospheres generated from the β-gal$^+$ and β-gal$^-$ cortical cells after culturing for 7 DIV in the neurosphere media. Error bars show SD. *Significant difference, $p < 0.0001$.

(F) Efficient Notch signaling from the Mib1-expressing cortical cells. The wild-type (positive control) and *Nestin-cre;mib1*$^{f/f}$ (negative control) cortical cells before FDG sorting and the β-gal$^+$ and β-gal$^-$ cortical cells after FDG sorting were cocultured with N1-C2C12 cells transfected with the wild-type (white bars) and mutant (black bars) Hes1-Luc vectors. At 24 hr after coculture, the luciferase activity was measured. Error bars show SD. *Significant difference, $p < 0.0001$.

Newly generated IPs and neurons express Mib1 in a specific phase of their migration. Because *mib1* was colocalized with *tbr2* and *dll1* in the basal region of the VZ and in the SVZ and because the *mib1* promoter was not active in MAP2$^+$ cells in the CP, its expression is restricted in the migrating IPs and postmitotic neurons to the CP. These Mib1-expressing cells are able to generate Notch signaling to the neighboring cells, and the cortical cells from the mutant neocortexes failed to send Notch signals, despite the fact that IPs and neurons were dramatically increased in the mutant brains. These data indicate that Mib1-expressing IPs and neurons are critical for the generation of Notch signaling to RGCs. Indeed, a histological analysis of the *Nestin-cre;mib1*$^{f/f}$ and *hGFAP-cre;mib1*$^{f/f}$ neocortexes and DiI labeling experiments showed that a dividing RGC at the VS prematurely differentiated through abnormal symmetric division (N-N or IP-IP division) instead of the proper asymmetric division retaining the RGCs. This premature differentiation was reverted by expressing N1ICD in the *hGFAP-cre;Rosa-Notch1* mice, indicating that the activation of Notch signaling by Mib1-expressing migratory IPs or neurons is essential for proper asymmetric division of the RGCs in the VS.

In addition to asymmetric division, RGCs also divide symmetrically to expand their pool (Guillemot, 2005). These RGCs also definitely require Notch signaling to maintain their stemness during symmetric division, because they were depleted in the *Nestin-cre;mib1*$^{f/f}$ and hGFAP-*cre;mib1*$^{f/f}$ mice. However, how can Notch signaling be activated in the symmetrically dividing RGCs, which do not produce neuronal daughters expressing Mib1? In the present study, we show that RGCs can interact with Mib1-expressing IPs and postmitotic neurons generated by asymmetric division of the neighboring RGCs to get Notch signaling, suggesting that these interactions could be an efficient strategy to control both the asymmetric and symmetric divisions of RGCs (Figure 7G).

According to time-lapse imaging, the newly generated IPs or neurons remain in the VZ or SVZ for more than 24 hr and show retrograde movement toward the VS until the next division of parental RGCs is completed (Noctor et al., 2004). In this study, the expression of the Notch ligands and Mib1 was rarely detectable in the RGCs before and during the asymmetric division at the VS. Thus, IPs or neurons right after S-Div of RGCs would not be ready to activate Notch signaling to a stem cell daughter, due to the low expression of the Notch ligands and Mib1. During the migration to the SVZ, however, it becomes competent to activate Notch signaling in a sibling RGC by expressing the Notch ligands, which become activated by Mib1. Because RGCs

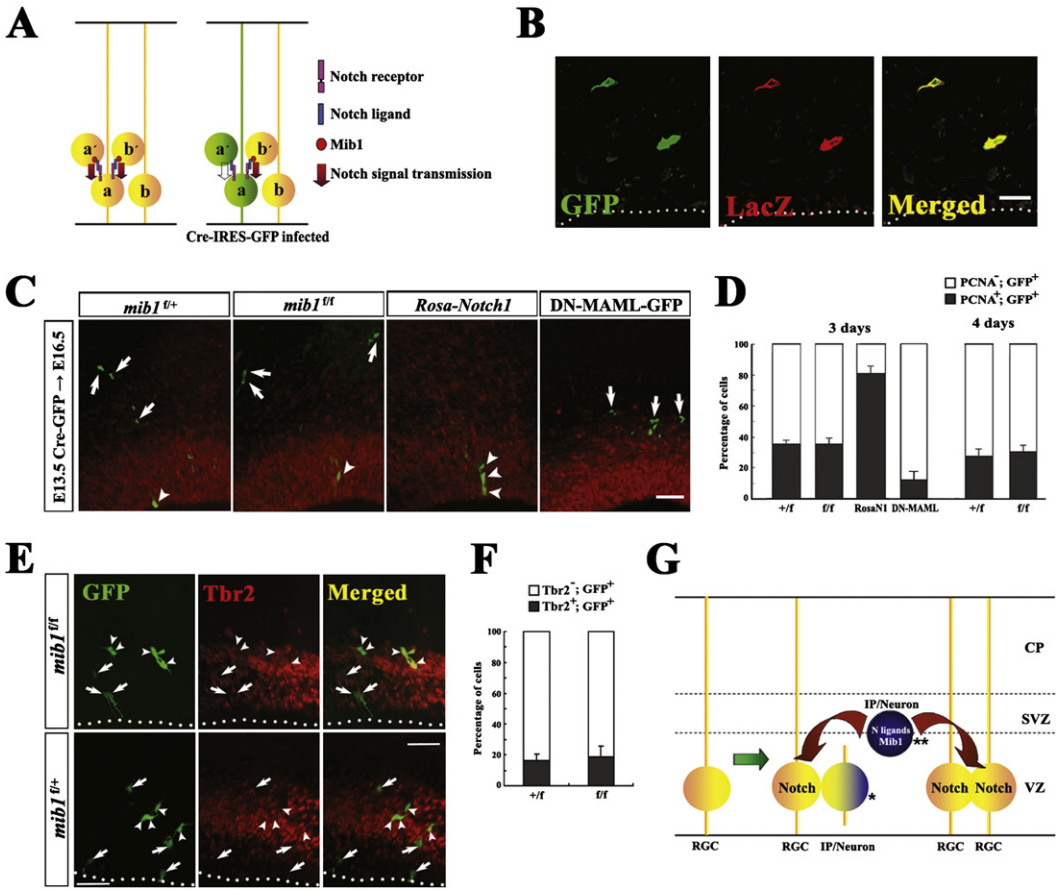

Figure 7. RGCs Can Interact with the Mib1-Expressing IPs and Postmitotic Neurons Generated by Neighboring RGCs to Get Notch Signaling

(A) Left panel. Notch signaling between an RGC and its own daughter cell or between an RGC and a daughter cell produced by a neighboring RGC. It is possible that an RGC (a) can receive the Notch signal from its own daughter cell (á, a clonal daughter cell) or a daughter cell that originated from other surrounding RGCs (b́, a nonclonal daughter cell). Notch receptors (pink rectangles), Notch ligands (blue rectangles), and Mib1 (red circles) are depicted. Red arrows represent the transmission of the Notch signal. Right panel. A schematic illustration of the effects of the Cre-IRES-GFP retrovirus infection on the *mib1*$^{f/f}$ brain. Due to the clonal deletion of Mib1 by Cre recombinase in the infected GFP$^+$ cells (green), the daughter cells derived from the infected RGCs (á) are unable to send the Notch signal to the parental RGCs (a). Therefore, the GFP$^+$ RGCs can receive the Notch signal only from nonclonal daughters (b́). The empty arrow represents the absence of Notch signaling.

(B) Cre-IRES-GFP retrovirus-mediated genomic recombination at 24 hr after in utero infection. The section of the Cre-IRES-GFP-infected *Rosa26R* reporter embryos was stained with anti-GFP (left panel) and anti-β-galactosidase (middle panel) antibodies. The merged image (right panel) shows that the Cre-IRES-GFP-infected cells have already experienced the Cre-mediated genomic recombination at 24 hr after the retroviral infection. Scale bar: 20 μm.

(C) The result of GFP (in green) and PCNA (in red) immunohistochemistry on the frozen sections of the neocortex in the Cre-IRES-GFP and DN-MAML-GFP retrovirus-infected embryos at 3 days after in utero infection. The infected cells in the *mib1*$^{+/f}$ brain, as well as those in the *mib1*$^{f/f}$ brain, reside in both the proliferating zone (the VZ and the SVZ) (arrowheads, GFP$^+$/PCNA$^+$) and the neuronal layer (arrows, GFP$^+$/PCNA$^-$). The infected cells in the *Rosa-Notch1* brain reside predominantly in the VZ (arrowheads, GFP$^+$/PCNA$^+$), suggesting that the overactivation of Notch signaling leads to the symmetric proliferative division, which cannot produce neurons. In contrast, the DN-MAML-GFP retrovirus-infected cells are mainly PCNA$^-$ (arrows). Scale bar: 50 μm.

(D) The percentage of proliferating cells and cell cycle exiting cells in Cre-IRES-GFP and DN-MAML-GFP retrovirus-infected cells at 3 or 4 days after infection. Although the proliferating cells are dramatically increased in the *Rosa-Notch1* brain and decreased in the DN-MAML-GFP retrovirus-infected brain, there is no significant difference between the *mib1*$^{+/f}$ and *mib1*$^{f/f}$ brains. Error bars show SD.

(E) The results of GFP (in green) and Tbr2 (in red) immunohistochemistry on the frozen sections of the neocortex in the Cre-IRES-GFP retrovirus-infected embryos at 3 days after in utero infection. Arrowheads and arrows represent Tbr2$^+$/GFP$^+$ cells and Tbr2$^-$/GFP$^+$ cells, respectively. The dotted lines indicate the ventricular surface. Scale bar: 50 μm.

(F) The percentages of Tbr2$^+$ and Tbr2$^-$ cells in the Cre-IRES-GFP retrovirus-infected cells at 3 days after the infection. There is no significant difference in the number of retrovirus-infected IPs between the *mib1*$^{+/f}$ and *mib1*$^{f/f}$ brains. Error bars show SD.

(G) The modes of Notch signal transmission in asymmetric and symmetric divisions of RGCs. Mib1 is expressed predominantly in the migrating IPs or neurons and activates the Notch ligands, such as Dll1 and Dll3. IPs or neurons right after RGC divisions at the ventricular surface (asterisk) might be incompetent to send the Notch signal, due to the low expression of Mib1 and Notch ligands. After asymmetric division, Mib1-expressing signal-sending competent IPs or neurons (double asterisk) can send the Notch signal to clonal and nonclonal RGCs. After symmetric proliferative division, only nonclonal IPs and neurons can send Notch signaling to RGCs, which is essential for the maintenance of RGCs. VZ, the ventricular zone; SVZ, the subventricular zone; CP, the cortical plate.

definitely need the Notch signal to maintain their stemness (Anthony et al., 2005; Gaiano et al., 2000; Yoon et al., 2004), it is plausible that the competent neuronal daughters delay their basal migration and spend several hours in the vicinity of the parental RGCs to send the Notch signal efficiently, until the next division of the parental RGCs is completed and the next daughters become competent again. Therefore, the Notch-signal-sending competent IPs and neurons ensure that the RGCs can divide repetitively to produce new IPs and neurons while maintaining their stemness. Because the rate of neuronal daughter generation at the VS progressively decreases in the late stage of neurogenesis (Takahashi et al., 1995), the number of signal-sending neuronal daughters in the VZ and the SVZ might decrease. Thus, the decreased generation of competent neuronal daughters near the soma of RGCs might result in the reduction of Notch signaling activity in the RGCs (Tokunaga et al., 2004), which finally depletes the RGCs after birth.

In slice culture experiments, bipolar RGCs showed two different patterns of aberrant division in the absence of Notch signaling. RGCs lacking the pial process divided at the surface, and their daughter cells became neurons, while RGCs without the apical attachment became two IPs after surface division. In slices derived from the *mib1*-null brains, bipolar RGCs showed two different patterns of aberrant division in the absence of Notch signaling. RGCs lacking the pial process divided at the surface, and their daughter cells became neurons, while RGCs without the apical attachment became two IPs after surface division. It is unclear how the basal attachment of the RGC in the *mib1*-null cortices can influence the fate of the daughter cell, although it is dispensable for the fate determination of the RGCs (Haubst et al., 2006). Meanwhile, the importance of the apical attachment of the RGC in the daughter cell fate is still controversial, because the ablations of *cdc42* (Cappello et al., 2006) and *aPKClambda* (Imai et al., 2006), which are molecules regulating the adherens junction at the VS, yielded different results. Therefore, it is interesting to examine (1) the role of the basal and apical attachments of the RGC in the fate of the daughter cell and (2) the role of Notch signaling in the maintenance of the basal and apical attachments of the RGC.

In conclusion, Mib1 is an essential regulator for generating Notch signaling from migrating neuronal daughters to RGCs in mammalian neurogenesis. The continuous Notch activation by migrating Mib1$^+$ IPs and neurons ensures the maintenance of radial glial identity during repetitive RGC divisions in the neurogenic stage of the developing brain. Our study provides a mechanism for the maintenance of RGCs during symmetric and asymmetric divisions.

EXPERIMENTAL PROCEDURES

Mice

The floxed (f) allele of *mib1* was generated previously (Koo et al., 2007). The *Nestin-cre* and *hGFAP-cre* transgenic mice and the *Rosa26R* reporter mice (Soriano, 1999) were obtained from Jackson Laboratory. The *Rosa-Notch1* mice and the TNR mice were kind gifts from Dr. Douglas Melton (Harvard University) and Dr. Nicholas Gaiano (Johns Hopkins University), respectively. The *Nestin-cre;mib1*$^{f/f}$ and *hGFAP-cre; mib1*$^{f/f}$ mice were generated by mating the *mib1*$^{f/f}$ mice with the *Nestin-cre;mib1*$^{+/f}$ and *hGFAP-cre;mib1*$^{+/f}$ mice, respectively.

Slice Culture and DiI Labeling Experiment

Coronal slices were prepared from embryos generated by mating the *mib1*$^{f/f}$ mice with the *hGFAP-cre;mib1*$^{+/f}$ mice at E13.5 and were cultured in collagen gel as previously described (Miyata et al., 2001, 2004). Time-lapse recording was performed manually, as described previously (Miyata et al., 2004). Images were taken using Zeiss Axioskop2 Plus microscopy. Cultured slices were fixed in 4% paraformaldehyde for 10 min, vibratome-sectioned, treated with antibodies, and subjected to Olympus FV1000 confocal microscopy, as described (Miyata et al., 2004).

Fluorescein Digalactopyranoside-Mediated Cell Sorting, Neurosphere-Forming Assay, and Luciferase Assay

Fluorescein digalactopyranoside (FDG) sorting was performed as described (Nieto et al., 2001). Briefly, cortices were isolated from the E13.5 *mib1*$^{+/LacZ}$ and *mib1*$^{+/+}$ embryos (Koo et al., 2005) and were dissociated by papain (Worthington Biochemical Corporation). Embryos were typed by X-gal staining during the dissociation process. Dissociated cells were filtered though a 70 μm cell strainer (BD Falcon) and were stained with FDG by osmotic shock (1 min, 37°C), according to the manufacturer's protocol (Molecular Probes). To sort out the dead cells during the procedure, propidium iodide was added to the staining medium before the sorting. FDG-labeled cells from *mib1*$^{+/+}$ cortices served as negative controls. Efficient separation of the β-gal$^+$ and β-gal$^-$ populations was assessed by FACS analysis. We routinely obtained < 1% of contaminating β-gal$^-$ cells in the β-gal$^+$ population (data not shown). The CD133/EGFP sorting of TNR cortical cells was performed as previously described (Mizutani et al., 2007). All sorts and analyses were performed on a FACS Vantage SE (BD Biosciences). Neurospheres were generated from the sorted cells as described (Grandbarbe et al., 2003). Stable C2C12 cell lines expressing Notch1 (N113) (kindly provided by Dr. Gerry Weinmaster, UCLA) (Nofziger et al., 1999) were transfected with Hes-1-luc or Hes-1-ΔABluc constructs (Jarriault et al., 1995) (kindly provided by Dr. Alain Israel, Institut Pasteur) and pRL-TK using the Lipofectamine Plus Reagent (Invitrogen) and were cultured for 24 hr. They were then cocultured with the sorted β-gal$^+$ or β-gal$^-$ cortical cells for 24 hr, and the luciferase activities were subsequently measured with a Dual Luciferase Kit (Promega). Cortical cells from the wild-type and *Nestin-cre;mib1*$^{f/f}$ brains without the sorting were used as positive and negative controls, respectively.

In Utero Cre-IRES-GFP Retrovirus Infection

The plasmids for the generation of the Cre-IRES-GFP and DN-MAML-GFP retroviruses were kindly provided by Dr. Jinfang Zhu (NIAID) and Dr. J.C. Aster (Brigham and Women's Hospital, Harvard Medical School), respectively. The method of retrovirus production was described previously (Yoon et al., 2004). The concentrated retrovirus was injected into the lateral ventricles of E13.5 embryos by in utero surgery.

SUPPLEMENTAL DATA

The Supplemental Data for this article can be found online at http://www.neuron.org/cgi/content/full/58/4/519/DC1/.

ACKNOWLEDGMENTS

We thank the members of Professor Kong's lab for discussions; Dr. Keejung Yoon for carefully reading the manuscript; Dr. Jaesang Kim for helpful comments; Dr. Joung-Hun Kim, Dr. Haeyoung Suh-Kim, and Rae-Hee Park for technical support; and Dr. Robert F. Hevner, Dr. Patricia J. Gallagher, Dr. Douglas Melton, Dr. Jinfang Zhu, Dr. Alain Israel, Dr. Gerry Weinmaster, and Dr. Nicholas Gaiano for their kind material transfer. This research was supported by a grant (M103KV010021-06K2201-02110) from the Brain Research Center of the 21st Century Frontier Research Program, funded by the Ministry of Science and Technology, the Republic of Korea.

Received: August 2, 2007
Revised: December 23, 2007
Accepted: March 18, 2008
Published: May 21, 2008

REFERENCES

Aaku-Saraste, E., Hellwig, A., and Huttner, W.B. (1996). Loss of occludin and functional tight junctions, but not ZO-1, during neural tube closure–remodeling of the neuroepithelium prior to neurogenesis. Dev. Biol. *180*, 664–679.

Anthony, T.E., Klein, C., Fishell, G., and Heintz, N. (2004). Radial glia serve as neuronal progenitors in all regions of the central nervous system. Neuron *41*, 881–890.

Anthony, T.E., Mason, H.A., Gridley, T., Fishell, G., and Heintz, N. (2005). Brain lipid-binding protein is a direct target of Notch signaling in radial glial cells. Genes Dev. *19*, 1028–1033.

Bardin, A.J., Le Borgne, R., and Schweisguth, F. (2004). Asymmetric localization and function of cell-fate determinants: a fly's view. Curr. Opin. Neurobiol. *14*, 6–14.

Campos, L.S., Duarte, A.J., Branco, T., and Henrique, D. (2001). mDll1 and mDll3 expression in the developing mouse brain: role in the establishment of the early cortex. J. Neurosci. Res. *64*, 590–598.

Cappello, S., Attardo, A., Wu, X., Iwasato, T., Itohara, S., Wilsch-Brauninger, M., Eilken, H.M., Rieger, M.A., Schroeder, T.T., Huttner, W.B., et al. (2006). The Rho-GTPase cdc42 regulates neural progenitor fate at the apical surface. Nat. Neurosci. *9*, 1099–1107.

Englund, C., Fink, A., Lau, C., Pham, D., Daza, R.A., Bulfone, A., Kowalczyk, T., and Hevner, R.F. (2005). Pax6, Tbr2, and Tbr1 are expressed sequentially by radial glia, intermediate progenitor cells, and postmitotic neurons in developing neocortex. J. Neurosci. *25*, 247–251.

Gaiano, N., Nye, J.S., and Fishell, G. (2000). Radial glial identity is promoted by Notch1 signaling in the murine forebrain. Neuron *26*, 395–404.

Grandbarbe, L., Bouissac, J., Rand, M., Hrabe de Angelis, M., Artavanis-Tsakonas, S., and Mohier, E. (2003). Delta-Notch signaling controls the generation of neurons/glia from neural stem cells in a stepwise process. Development *130*, 1391–1402.

Graus-Porta, D., Blaess, S., Senften, M., Littlewood-Evans, A., Damsky, C., Huang, Z., Orban, P., Klein, R., Schittny, J.C., and Muller, U. (2001). Beta1-class integrins regulate the development of laminae and folia in the cerebral and cerebellar cortex. Neuron *31*, 367–379.

Guillemot, F. (2005). Cellular and molecular control of neurogenesis in the mammalian telencephalon. Curr. Opin. Cell Biol. *17*, 639–647.

Hartfuss, E., Galli, R., Heins, N., and Gotz, M. (2001). Characterization of CNS precursor subtypes and radial glia. Dev. Biol. *229*, 15–30.

Haubst, N., Georges-Labouesse, E., De Arcangelis, A., Mayer, U., and Gotz, M. (2006). Basement membrane attachment is dispensable for radial glial cell fate and for proliferation, but affects positioning of neuronal subtypes. Development *133*, 3245–3254.

Huttner, W.B., and Kosodo, Y. (2005). Symmetric versus asymmetric cell division during neurogenesis in the developing vertebrate central nervous system. Curr. Opin. Cell Biol. *17*, 648–657.

Imai, F., Hirai, S., Akimoto, K., Koyama, H., Miyata, T., Ogawa, M., Noguchi, S., Sasaoka, T., Noda, T., and Ohno, S. (2006). Inactivation of aPKClambda results in the loss of adherens junctions in neuroepithelial cells without affecting neurogenesis in mouse neocortex. Development *133*, 1735–1744.

Itoh, M., Morita, K., and Tsukita, S. (1999). Characterization of ZO-2 as a MAGUK family member associated with tight as well as adherens junctions with a binding affinity to occludin and alpha catenin. J. Biol. Chem. *274*, 5981–5986.

Itoh, M., Kim, C.H., Palardy, G., Oda, T., Jiang, Y.J., Maust, D., Yeo, S.Y., Lorick, K., Wright, G.J., Ariza-McNaughton, L., et al. (2003). Mind bomb is a ubiquitin ligase that is essential for efficient activation of Notch signaling by Delta. Dev. Cell *4*, 67–82.

Jarriault, S., Brou, C., Logeat, F., Schroeter, E.H., Kopan, R., and Israel, A. (1995). Signalling downstream of activated mammalian Notch. Nature *377*, 355–358.

Jarriault, S., Le Bail, O., Hirsinger, E., Pourquie, O., Logeat, F., Strong, C.F., Brou, C., Seidah, N.G., and Isra l, A. (1998). Delta-1 activation of notch-1 signaling results in HES-1 transactivation. Mol. Cell. Biol. *18*, 7423–7431.

Jesaitis, L.A., and Goodenough, D.A. (1994). Molecular characterization and tissue distribution of ZO-2, a tight junction protein homologous to ZO-1 and the Drosophila discs-large tumor suppressor protein. J. Cell Biol. *124*, 949–961.

Jin, Y., Blue, E.K., Dixon, S., Shao, Z., and Gallagher, P.J. (2002). A death-associated protein kinase (DAPK)-interacting protein, DIP-1, is an E3 ubiquitin ligase that promotes tumor necrosis factor-induced apoptosis and regulates the cellular levels of DAPK. J. Biol. Chem. *277*, 46980–46986.

Justice, N.J., and Jan, Y.N. (2002). Variations on the Notch pathway in neural development. Curr. Opin. Neurobiol. *12*, 64–70.

Koo, B.K., Lim, H.S., Song, R., Yoon, M.J., Yoon, K.J., Moon, J.S., Kim, Y.W., Kwon, M.C., Yoo, K.W., Kong, M.P., et al. (2005). Mind bomb 1 is essential for generating functional Notch ligands to activate Notch. Development *132*, 3459–3470.

Koo, B.K., Yoon, M.J., Yoon, K.J., Im, S.K., Kim, Y.Y., Kim, C.H., Suh, P.G., Jan, Y.N., and Kong, Y.Y. (2007). An obligatory role of mind bomb-1 in notch signaling of Mammalian development. PLoS ONE *2*, e1221.

Le Borgne, R., and Schweisguth, F. (2003). Unequal segregation of Neuralized biases Notch activation during asymmetric cell division. Dev. Cell *5*, 139–148.

Lindsell, C.E., Shawber, C.J., Boulter, J., and Weinmaster, G. (1995). Jagged: a mammalian ligand that activates Notch1. Cell *80*, 909–917.

Malatesta, P., Hack, M.A., Hartfuss, E., Kettenmann, H., Klinkert, W., Kirchhoff, F., and Gotz, M. (2003). Neuronal or glial progeny: regional differences in radial glia fate. Neuron *37*, 751–764.

Miyata, T. (2007). Asymmetric cell division during brain morphogenesis. Prog. Mol. Subcell. Biol. *45*, 121–142.

Miyata, T., Kawaguchi, A., Okano, H., and Ogawa, M. (2001). Asymmetric inheritance of radial glial fibers by cortical neurons. Neuron *31*, 727–741.

Miyata, T., Kawaguchi, A., Saito, K., Kawano, M., Muto, T., and Ogawa, M. (2004). Asymmetric production of surface-dividing and non-surface-dividing cortical progenitor cells. Development *131*, 3133–3145.

Mizutani, K., Yoon, K., Dang, L., Tokunaga, A., and Gaiano, N. (2007). Differential Notch signalling distinguishes neural stem cells from intermediate progenitors. Nature *449*, 351–355.

Murtaugh, L.C., Stanger, B.Z., Kwan, K.M., and Melton, D.A. (2003). Notch signaling controls multiple steps of pancreatic differentiation. Proc. Natl. Acad. Sci. USA *100*, 14920–14925.

Nieto, M., Schuurmans, C., Britz, O., and Guillemot, F. (2001). Neural bHLH genes control the neuronal versus glial fate decision in cortical progenitors. Neuron *29*, 401–413.

Noctor, S.C., Flint, A.C., Weissman, T.A., Dammerman, R.S., and Kriegstein, A.R. (2001). Neurons derived from radial glial cells establish radial units in neocortex. Nature *409*, 714–720.

Noctor, S.C., Martinez-Cerdeno, V., Ivic, L., and Kriegstein, A.R. (2004). Cortical neurons arise in symmetric and asymmetric division zones and migrate through specific phases. Nat. Neurosci. *7*, 136–144.

Nofziger, D., Miyamoto, A., Lyons, K.M., and Weinmaster, G. (1999). Notch signaling imposes two distinct blocks in the differentiation of C2C12 myoblasts. Development *126*, 1689–1702.

Pavlopoulos, E., Pitsouli, C., Klueg, K.M., Muskavitch, M.A., Moschonas, N.K., and Delidakis, C. (2001). neuralized Encodes a peripheral membrane protein involved in delta signaling and endocytosis. Dev. Cell *1*, 807–816.

Rhyu, M.S., Jan, L.Y., and Jan, Y.N. (1994). Asymmetric distribution of numb protein during division of the sensory organ precursor cell confers distinct fates to daughter cells. Cell *76*, 477–491.

Ruan, Y., Tecott, L., Jiang, M.M., Jan, L.Y., and Jan, Y.N. (2001). Ethanol hypersensitivity and olfactory discrimination defect in mice lacking a homolog of Drosophila neuralized. Proc. Natl. Acad. Sci. USA *98*, 9907–9912.

Soriano, P. (1999). Generalized lacZ expression with the ROSA26 Cre reporter strain. Nat. Genet. *21*, 70–71.

Spana, E.P., and Doe, C.Q. (1996). Numb antagonizes Notch signaling to specify sibling neuron cell fates. Neuron *17*, 21–26.

Takahashi, T., Nowakowski, R.S., and Caviness, V.S., Jr. (1995). The cell cycle of the pseudostratified ventricular epithelium of the embryonic murine cerebral wall. J. Neurosci. *15*, 6046–6057.

Tokunaga, A., Kohyama, J., Yoshida, T., Nakao, K., Sawamoto, K., and Okano, H. (2004). Mapping spatio-temporal activation of Notch signaling during neurogenesis and gliogenesis in the developing mouse brain. J. Neurochem. *90*, 142–154.

Tronche, F., Kellendonk, C., Kretz, O., Gass, P., Anlag, K., Orban, P.C., Bock, R., Klein, R., and Schutz, G. (1999). Disruption of the glucocorticoid receptor gene in the nervous system results in reduced anxiety. Nat. Genet. *23*, 99–103.

Vollrath, B., Pudney, J., Asa, S., Leder, P., and Fitzgerald, K. (2001). Isolation of a murine homologue of the Drosophila neuralized gene, a gene required for axonemal integrity in spermatozoa and terminal maturation of the mammary gland. Mol. Cell. Biol. *21*, 7481–7494.

Weng, A.P., Nam, Y., Wolfe, M.S., Pear, W.S., Griffin, J.D., Blacklow, S.C., and Aster, J.C. (2003). Growth suppression of pre-T acute lymphoblastic leukemia cells by inhibition of notch signaling. Mol. Cell. Biol. *23*, 655–664.

Yoon, K., and Gaiano, N. (2005). Notch signaling in the mammalian central nervous system: insights from mouse mutants. Nat. Neurosci. *8*, 709–715.

Yoon, K., Nery, S., Rutlin, M.L., Radtke, F., Fishell, G., and Gaiano, N. (2004). Fibroblast growth factor receptor signaling promotes radial glial identity and interacts with Notch1 signaling in telencephalic progenitors. J. Neurosci. *24*, 9497–9506.

Zhuo, L., Theis, M., Alvarez-Maya, I., Brenner, M., Willecke, K., and Messing, A. (2001). hGFAP-cre transgenic mice for manipulation of glial and neuronal function in vivo. Genesis *31*, 85–94.